



Effect of graphene functionalizing on the performance of NiMo/graphene in HDS and HDN reactions

Babak Behnejad¹ · Majid Abdouss¹ · Ahmad Tavasoli²

Received: 2 September 2018
© The Author(s) 2019

Abstract

In this research, to remove sulfur and nitrogen compounds from heavy naphtha, various nanocatalysts were prepared through supporting NiMo over nanoporous graphene and evaluated in hydrodesulfurization and hydrodenitrogenation reactions. The nanoporous graphene was initially functionalized in order to facilitate the metal being loaded on it. Three different methods were used to functionalize the nanoporous graphene. The NiMo/nanoporous graphene nanocatalysts were characterized by field emission scanning electron microscopy, Fourier transform infrared spectroscopy, X-ray diffraction, inductively coupled plasma optical emission spectrometry, temperature-programmed reduction, nitrogen adsorption–desorption isotherms and transmission electron microscopy techniques. Catalyst performance was evaluated in terms of conversions of sulfur, mercaptans (R-SH) and nitrogen compounds. It was found that the functionalized nanoporous graphene support could significantly enhance the catalytic performance in comparison with the industrial NiMo/alumina catalyst. Among the functionalized graphene supports, amine-functionalized graphene exhibited the best results. By using NiMo supported over amine-functionalized graphene, the conversions of total sulfur and R-SH reached 97.8% and 98.1%, respectively.

Keywords Hydrodesulfurization (HDS) · Hydrotreating (HDT) · Nanocatalyst · Catalyst support · Graphene functionalization · NiMo/nanoporous graphene

1 Introduction

Catalyst support has a great effect on the performance of the catalyst, and the development of new and more effective supports is an important issue (Andonova et al. 2007; Dhar et al. 2003; Gutiérrez et al. 2014; Mendoza-Nieto et al. 2015). The active phases of the catalysts are distributed over the support materials to improve the activity and exposure of the active sites to the target molecules. The main catalyst supports include Al₂O₃ (Ayala-Gomez et al. 2015; Escobar et al. 2017; Nikulshin et al. 2014), SiO₂ (Xu et al. 2017), MgO (Zdražil 2003) and TiO₂ (Saih et al. 2005; Santes et al. 2004), with low specific surface area and low pore volume.

To tackle this problem of low specific surface area and low pore volume, carbon-based nanostructures including carbon nanotubes (CNTs) (Soghrati et al. 2012), nanoporous graphene (Hajjar et al. 2015, 2016, 2017) and active carbon (Nikulshin et al. 2014) have been considered as graphene supports. The nanocarbon materials possess high surface area and pore volume, which leads to better distribution of the catalyst active sites and hence can enhance the catalytic activity.

The successful hydrotreating (HDT) catalysts are composed of the active phase and the catalyst support, where NiMo (Escobar et al. 2017; Liu et al. 2016; Xu et al. 2017; Zepeda et al. 2016; Zhou et al. 2017) and CoMo (Bui et al. 2015; Khorami and Kalbasi 2011; Vonortas and Papayannakos 2014; Zdražil 2003) have been the most studied active phases. Liu et al. (2016) studied the HDS of dibenzothiophene over ordered mesoporous NiMo/Al₂O₃ and reported that high HDS activity was observed for the Ni/Mo molar ratio of 1:1. Saih et al. (2005) studied the ultra-deep HDS of dibenzothiophene over NiMo/TiO₂-Al₂O₃ catalysts where the NiMo sulfide was supported over TiO₂-coated Al₂O₃. They have reported that the NiMo/TiO₂-Al₂O₃ catalysts have

Edited by Xiu-Qin Zhu and Xiu-Qiu Peng

✉ Babak Behnejad
babak_behnejad@aut.ac.ir

¹ Department of Chemistry, Amirkabir University of Technology, Tehran, Iran

² School of Chemistry, College of Science, University of Tehran, Tehran, Iran

better performance than the NiMo/Al₂O₃ catalysts (Saih et al. 2005). In research performed by Escobar et al. (2017), the NiMo/alumina catalyst was modified by citric acid and utilized for HDS of benzothiophene for which it was found that impregnation of the alumina by citric acid before the addition of the active phase yields the highest activity. Xu et al. (2017) synthesized the NiMo/SiO₂-Al₂O₃ HDS catalysts which showed high activity for HDS of 4,6-dimethyldibenzothiophene FCC diesel. Regarding the application of the CoMo active phase, Vonortas and Papayannakos (2014) studied the HDS of heavy gas oil by using CoMo/alumina in the presence of free fatty acids, where the oxygenated molecules had an adverse effect on HDT performance. In other researches, maleic acid was used for activation of CoMo/Al₂O₃ catalyst which showed high HDS catalytic activity (Bui et al. 2015).

Recently, carbon-based nanostructures have been considered as catalyst support in HDT applications. Yu et al. supported the Co/Ni/Mo metals over carbon nanofiber for HDS of thiophene where the Co metal over carbon nanofiber showed better performance than the Co(Ni)Mo catalysts. Khorami and Kalbasi (2011) investigated the HDS activity of CoMo supported on CNTs and found that multiwalled carbon nanotubes (MWCNTs) are a suitable support for HDS catalysts. Soghrati et al. (2012) prepared Co–Mo supported on CNT-coated cordierite monoliths for HDS of naphtha which decreased the sulfur content from 2670 to 53 ppm. Liu et al. synthesized MoS₂/graphene for HDS of carbonyl sulfide which yielded high catalytic efficiency (Liu et al. 2014). Furthermore, Hajjar et al. (2016) studied graphene-based catalysts for HDS of naphtha and diesel. Co/Mo supported over graphene showed significant performance and reduced the sulfur content of the diesel from 13,000 to 13 ppm (Hajjar et al. 2016).

Here, the effect of the functionalization process on HDS and HDN activity of the NiMo-supported nanoporous graphene has been investigated. In this regard, three different methods were followed to add the functional groups to nanoporous graphene, which facilitate the metal loading, and affect the dispersion of the catalyst active phase.

2 Experimental

2.1 Materials and methods

The nanoporous graphene was purchased from the Research Institute of Petroleum Industry (RIPI), National Iranian Oil Company, Iran. The chemicals used in this research include sulfuric acid 98%, nitric acid 30%, analytical-grade nickel nitrate hexahydrate (Ni(NO₃)₂·6H₂O), ethylenediamine, ammonium heptamolybdate tetrahydrate ((NH₄)₆Mo₇O₂₄·4H₂O) and dimethyl disulfide (DMDS)

which were supplied from Merck Chemical Co. In addition, argon and H₂ of analytical grade and also deionized water (DI) were used throughout the experiments.

2.2 Functionalizing methods

Three methods were followed to functionalize the graphene. In the first method, graphene powder was dissolved in a solution of H₂SO₄/HNO₃ acid with a H₂SO₄/HNO₃ ratio of 3:1 (by volume) to provide carboxylic agents and the sample prepared with this type of graphene was labeled as NiMo/G1. In the second method, vapor from H₂SO₄/HNO₃ acid with a ratio of 3:1 (by volume) was used to functionalize the graphene and the sample prepared with this type of graphene was labeled as NiMo/G2. In the third method, acid treatment was carried out once more on G2 graphene by using ethylenediamine. The nanocatalyst prepared with amine-functionalized graphene was named as NiMo/G3.

2.3 NiMo/Gx preparation

To prepare the nanoporous graphene-supported NiMo catalyst, the incipient wetness impregnation method was used in which ammonium heptamolybdate tetrahydrate was dissolved in DI water and the resulting solution was added to the functionalized graphene powder. After that, the wet nanoporous graphene powder was dried at 120 °C for 4 h with a heating rate of 1 °C/min. To add nickel, the same procedure was performed to prepare the NiMo/G1–NiMo/G3 samples, and finally, the calcination process was carried out at 350 °C for 4 h in argon atmosphere.

2.4 Characterization

Various methods were employed to characterize the prepared NiMo/Gx nanocatalysts. XRD (PHILIPS PW1730, Netherlands) was used to investigate crystalline phases. To study the morphology of the nanopowders, FE-SEM was utilized (TESCAN MIRA, Czech). The N₂ adsorption–desorption isotherms, BET specific surface area, total pore volume and pore size distribution were acquired by the BET Belsorp Mini instrument. The FTIR spectra of the functionalized graphenes were recorded on a Bruker device, made in Germany. To investigate the metal loading of the NiMo/G1–NiMo/G3 nanocatalysts, ICP-OES spectrometry was utilized (PerkinElmer, Optima 8000 Dual views). Finally, a Micromeritics Chemisorb 2750 was used to obtain the TPR curves. In addition, high-resolution micrographs were taken with a TEM (Philips CM120, Netherlands).

2.5 Catalytic reactions

The hydrotreating reactions were carried out in a fixed-bed stainless steel reactor in which the down flow direction was considered. The schematic of the experimental reactor setup is shown in Fig. 1.

To carry out the catalytic reactions, a reactor 10 mm in diameter and 450 mm in length was utilized. By adopting an HPLC pump (Knauer K-501), the feed was injected into the reactor and for controlling the injection of H₂ into the reactor, a Brooks 5850 mass flow controller (MFC) was employed. Furthermore, a backpressure valve was utilized to control the pressure of the reaction system. The required heat was supplied by an adjustable electrical heater. In addition, a temperature indicator controller (TIC WEST 3400) was adopted to monitor and adjust the temperature. In the catalyst evaluation experiment, 1 g of the catalyst was placed in the central segment of the reactor between two layers of carborundum filler and glass beads. After a leak check of all connections by nitrogen gas, the sweeping N₂ was switched to H₂ gas followed by reducing the pressure to the required level.

Before performing the experiments, the NiMo/G1–NiMo/G3 nanocatalysts were sulfided by dimethyl disulfide (DMDS) with the conventional industrial procedure as shown in Table 1. Two steps were employed in the sulfiding process. After the sulfiding operation of the NiMo/G1–NiMo/G3 nanocatalysts, heavy naphtha was fed to the reactor. The reaction conditions are as follows: temperature of 290 °C, pressure of 3.0 MPa, LHSV of 3.3 h⁻¹, H₂/HC of 100 NL/L and reaction time of 240 h.

Fig. 1 Schematic of the experimental reactor setup (MFC mass flow controller, TIC temperature indicator controller, CWS cooling water supply, CWR cooling water return)

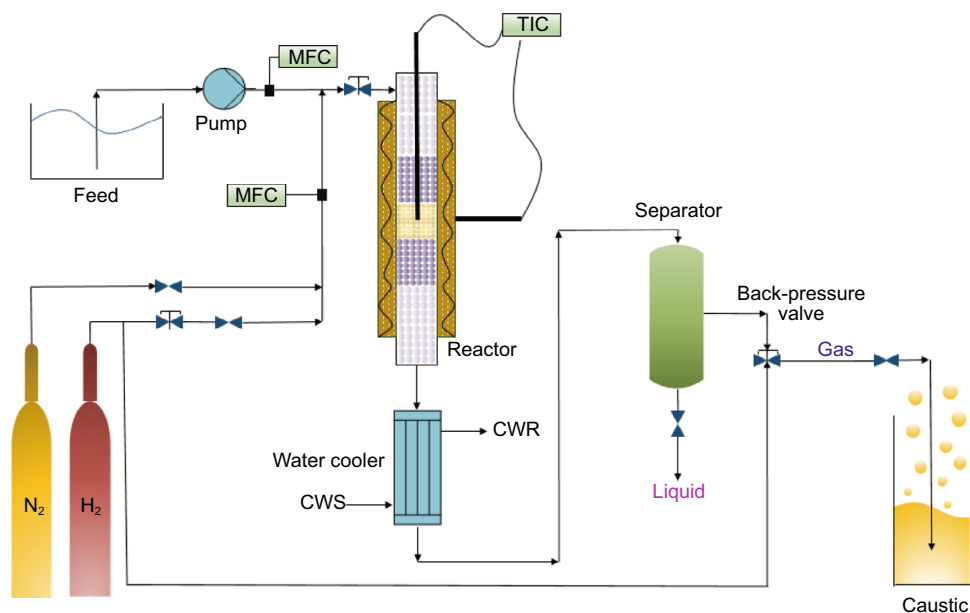


Table 1 Sulfiding conditions prior to HDS and HDN processes

Sulfiding conditions	Sulfiding (first step)	Sulfiding (second step)
Temperature, °C	220	330
Pressure, MPa	3.5	3.5
LHSV, h ⁻¹	3	3
H ₂ /HC, NL/L	115	115
Time, h	4	12

3 Results and discussion

3.1 Characterization

FTIR spectra of the functionalized graphene samples are shown in Fig. 2. The FTIR spectra were recorded after functionalizing the nanoporous graphene and before metal loading. The first two samples (i.e., G1 and G2) were functionalized by carboxylic groups. As it can be observed in the figure, the adsorption bands at 3427, 1634 and 1181 cm⁻¹ are related to O–H, C=N and C–O bonds, respectively. The FTIR spectrum of the sample which was carboxylic-functionalized by vapor shows absorption bands at 3424, 2922, 2854 and 804 cm⁻¹ which correspond to O–H, C–H, O–H, C=N and C=H bonds, respectively, and also the peaks at 1258 and 1114 cm⁻¹ indicate the formation of the C–H bond. Finally, in the FTIR spectrum of the amine-functionalized graphene, peaks at 3436, 2924, 1635 and 1124 cm⁻¹ were observed, and they are assigned to the NH, O–H, N–H and C–O bonds, respectively.

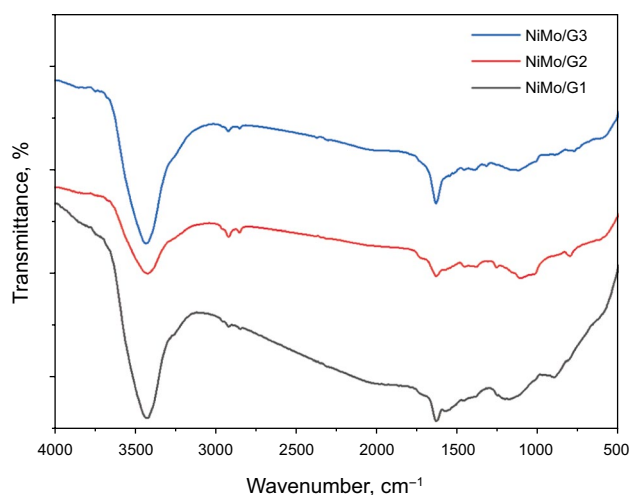


Fig. 2 FTIR spectra of the prepared NiMo/G_x samples

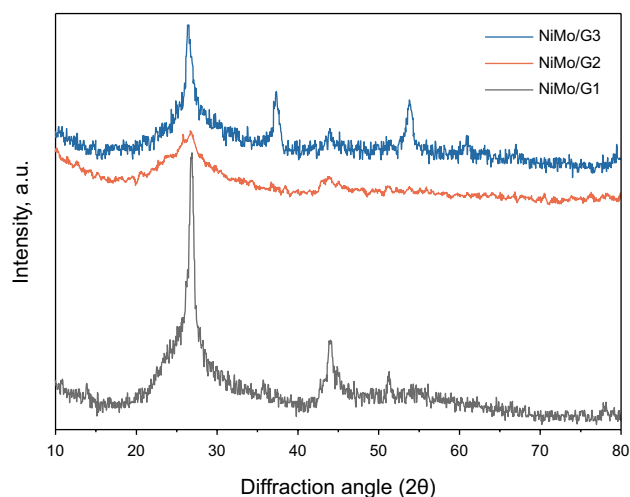


Fig. 3 XRD patterns of the prepared NiMo/G_x samples

The XRD patterns of the prepared NiMo/G_x samples are shown in Fig. 3. For all samples, the characteristic peak of the graphite phase is clear. For the NiMo/G1 sample, the peaks at 13.93° and 35.92° 2θ correspond to molybdenum oxide ($\text{Mo}_{18}\text{O}_{52}$, 01-074-1664) and the peaks at 26.83°, 44° and 51° are related to the carbon phase.

The XRD pattern of the NiMo/G2 sample shows peaks at 23.43° and 25.8°, indicating the formation of the MoO_3 crystalline phase (JCPDS 00-005-0508), and peaks at 26.7° and 43.8°, which show the carbon phase.

Finally, the NiMo/G3 sample has shown peaks at 2θ of 37°, 53° and 72° that are assigned to molybdenum oxide (JCPDS 00-001-0615) and peaks at 26.7° and 43°, which imply the presence of graphene support. All XRD patterns prove the formation of metal oxides over the nanoporous

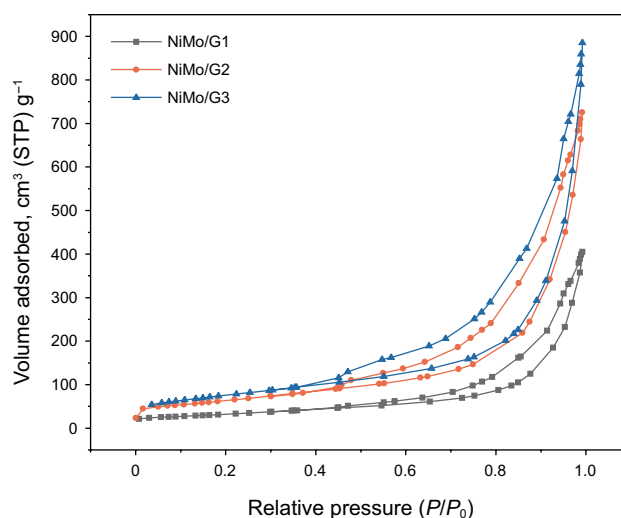


Fig. 4 Nitrogen adsorption–desorption isotherms of the NiMo/G_x samples

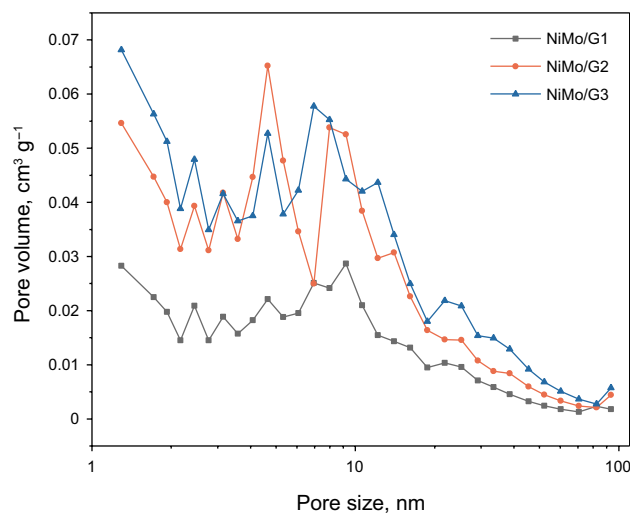


Fig. 5 Pore size distribution curves of the NiMo/G_x samples

graphene support that indicates the synthesis procedure has been performed successfully. However, it should be noted that due to the fact that only crystalline phases which are about 5 wt% can be detected by XRD techniques, the Ni-based phases could not be detected in XRD patterns of the samples.

The N_2 adsorption–desorption isotherms and pore size distribution curves of the prepared HDT nanocatalysts are shown in Figs. 4 and 5. As shown in Fig. 4, the same trend is observed for all samples, which have shown type 4 isotherms. As reported in the literature, the type 4 isotherm indicates the formation of mesoporous structures (Bell et al. 2001). As it is also evident from Fig. 5, all samples contain pores in the size range of mesopores.

The physical properties of the nanoporous graphene and samples are shown in Table 2, including BET specific surface area (S_{BET}), total pore volume, and mean pore diameter. The highest S_{BET} is obtained for the NiMo/G3 sample followed by NiMo/G2 and NiMo/G1 samples. The differences between the values obtained for S_{BET} of the samples might be due to different functionalizing processes where the optimum technique has provided the final support with less pore destruction. Therefore, the sample with better final surface characteristics had a higher specific surface area and pore volume, which can assist in catalytic activity. As it can be observed in Table 2, the NiMo/G3 sample has the highest total pore volume followed by NiMo/G2 and NiMo/G1. As a result, in terms of surface properties, the NiMo/G3 sample has shown the best performance regarding the BET surface area and total pore volume.

The FE-SEM micrographs of the NiMo/G1, NiMo/G2 and NiMo/G3 samples are shown in Figs. 6, 7 and 8, respectively. In the FE-SEM micrographs at two magnifications (with scale bars of 2 μm and 500 nm), the graphene support and the metal particles are clear for which there

are no major differences. The porous structure of the nanoporous graphene support which has been covered by metal oxides can be observed in these figures. Agglomeration of the metallic particles over the support is not observed, and the prepared catalysts can be more effective because of a suitable distribution of the active sites over the support that plays an important role in catalytic reactions.

Furthermore, the metal loading of each nanocatalyst is shown in Table 3. The NiMo/G3 has shown the highest total metal loading (i.e., 14.3 wt%), confirming the highest affinity of the amine-functionalized graphene toward metal adsorption. Also, the highest Ni/Mo mass ratio was obtained for NiMo/G3. NiMo/G1 and NiMo/G2 samples provided the Ni/Mo mass ratios of 0.22 and 0.25 and total metal loadings of 13.3 wt% and 13.5 wt%, respectively.

The TPR curves of the samples are shown in Fig. 9. As it can be observed in the figures, TPR curves of all samples are almost the same. For all samples, distinct continuous reduction peaks start at around 400 $^{\circ}\text{C}$ and end at around 700 $^{\circ}\text{C}$. The temperature range of 400–500 $^{\circ}\text{C}$ can be assigned to the reduction of molybdenum oxide and nickel oxide to form metal oxides with different oxidation states (Bunch and Ozkan 2002). In detail, Mo^{+6} is reduced to Mo^{+4} in this temperature range. Finally, by increasing the temperature, the oxide species are reduced and the pure metals are formed (Bunch and Ozkan 2002; Purón et al. 2017; Wang et al. 2015). The next peak in the TPR curve of the NiMo/G3 can be assigned for reducing the metal oxide to form pure metal which is distinct from those of other samples (Bunch and Ozkan 2002; Purón et al. 2017; Wang et al. 2015).

In order to study the distribution of the metal oxide nanoparticles over the nanoporous graphene, TEM images were

Table 2 Physical properties of the nanoporous graphene and prepared NiMo/Gx samples

Sample	S_{BET} , m^2/g	Total pore volume, cm^3/g	Mean pore diameter, nm
Nanoporous graphene	629.3	2.03	12.9
NiMo/G1	116.3	0.5974	20.546
NiMo/G2	228.58	1.0696	18.718
NiMo/G3	253.35	1.1167	18.535

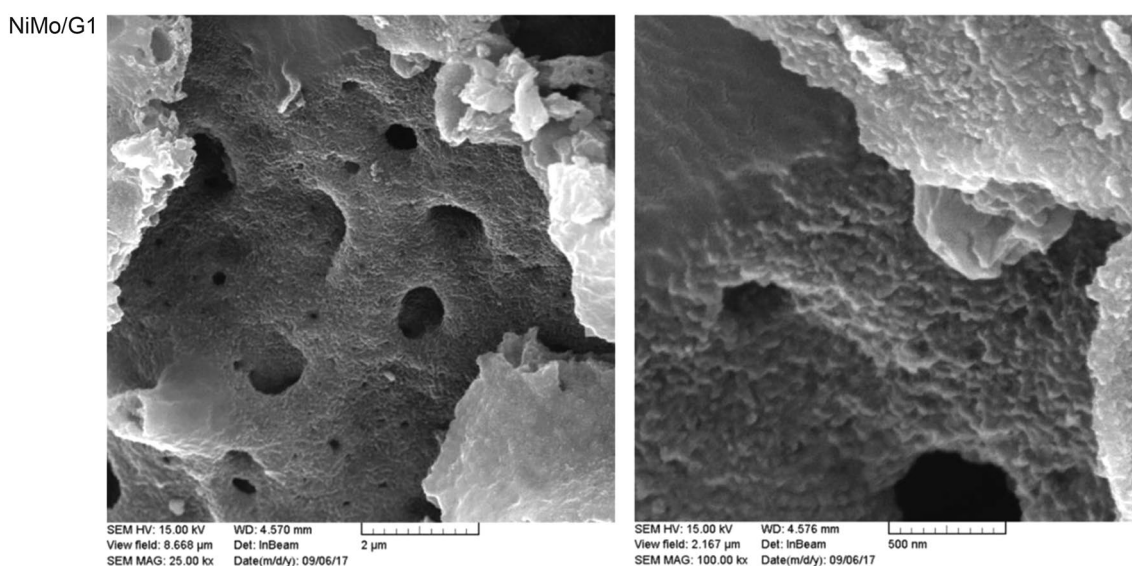


Fig. 6 FE-SEM micrographs of the NiMo/G1 sample at two magnifications

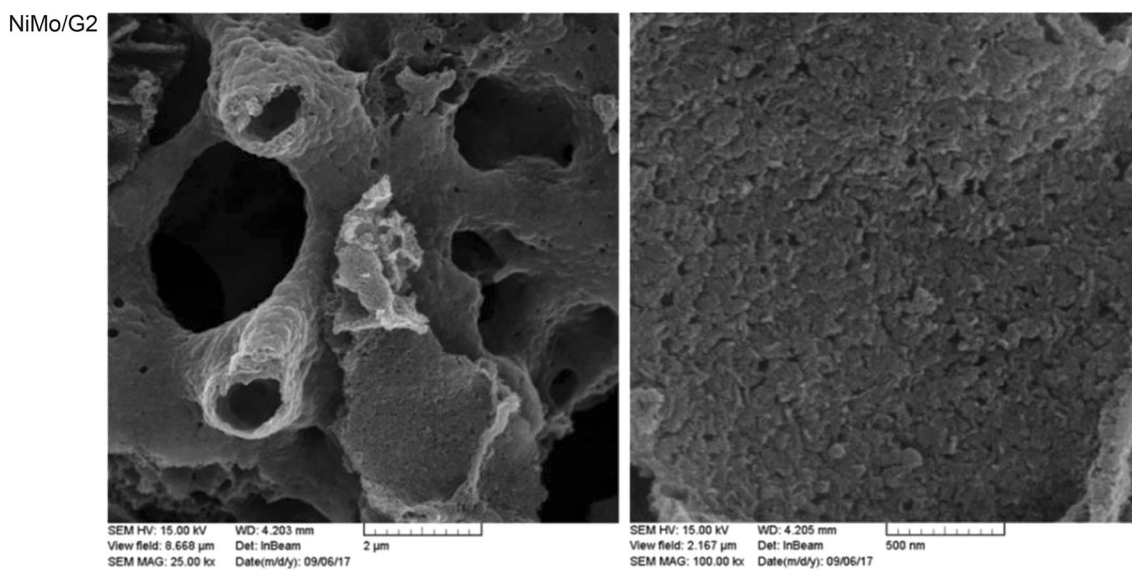


Fig. 7 FE-SEM micrographs of the NiMo/G2 sample at two magnifications

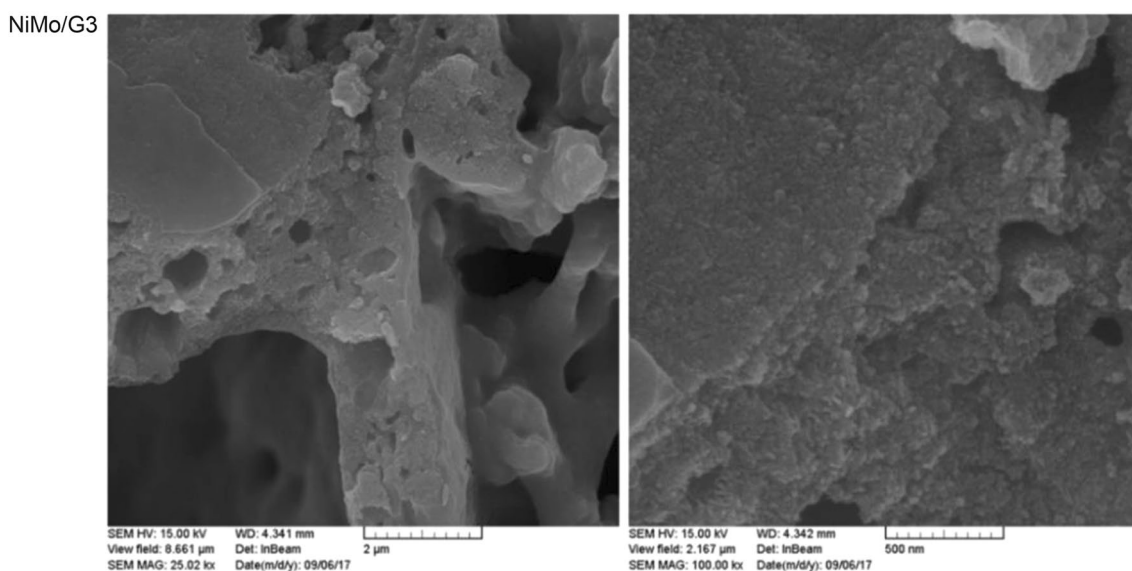


Fig. 8 FE-SEM micrographs of the NiMo/G3 sample at two magnifications

Table 3 Metal loading of the prepared NiMo/G_x samples and the industrial catalysts

Sample	Characteristic	
	ICP Ni/Mo (mass ratio)	ICP total metal loading, wt%
Industrial NiMo/Al ₂ O ₃	0.24	14.1
NiMo/G1	0.22	13.3
NiMo/G2	0.25	13.5
NiMo/G3	0.26	14.3

used. The TEM images of the NiMo/G3 sample are shown in Fig. 10, from which some points can be understood. At first, the graphene sheets which have been used as metal oxide support are clear in these figures. Further, it can be observed that metal oxide particles are uniformly distributed over the nanoporous graphene. As the catalytic activity of the active sites is a function of size and distribution of the particles, for synthesizing a catalyst with optimum performance, they should be controlled. The darker points over the nanoporous graphene correspond to metal oxide nanoparticles. From the

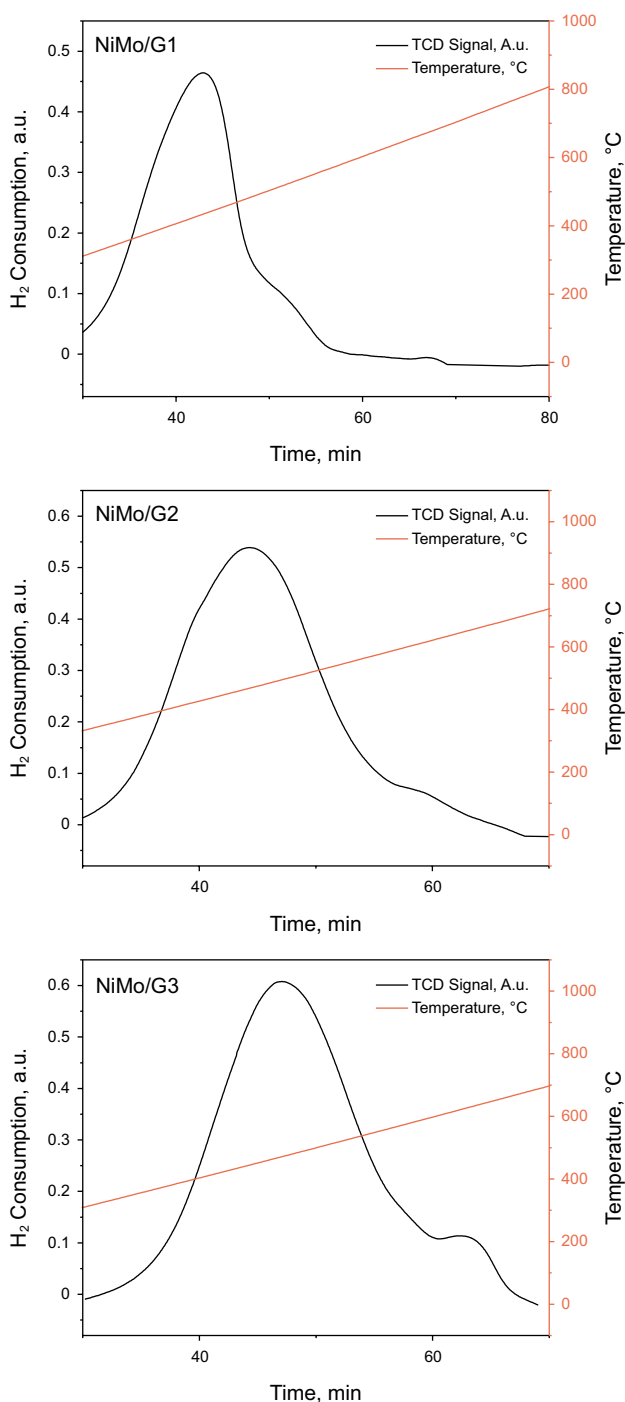


Fig. 9 TPR curves of the prepared NiMo/Gx nanocatalysts

figures, it can be understood that the metal oxide particles are in nanometer scale, which increases their overall catalytic activity. In addition, regarding the distribution of the particles, no agglomeration of the active sites is observed, which contributes to the high performance of the prepared nanocatalyst. These can be attributed to the functionalizing method of the NiMo/G3 sample that prevented the

agglomeration of particles and led to their uniform distribution in the nanometric scale.

3.2 Catalytic performance evaluation

The catalytic performance of the prepared NiMo/Gx nanocatalysts in HDS and HDN of heavy naphtha was studied. In addition, to get a deeper insight, the performance of the nanocatalysts was compared with that of the commercial NiMo/ γ -alumina catalyst. In this regard, the physical properties of the heavy naphtha feedstock were investigated before and after hydrotreating experiments. Feedstock specifications including specific gravity, research octane number (RON), total sulfur (TS), R-SH compounds (mercaptans) and total nitrogen (TN) are given in Table 4.

Considering the fact that the reaction system should be stable before taking samples in a steady-state condition, the samples were taken after the first 24 h. The ASTM D-86 test was performed on heavy naphtha feedstock and the products (after the first 24 h) of the NiMo/G1–NiMo/G3 catalysts and the industrial NiMo/ γ -alumina catalyst. As can be observed in Fig. 11, almost the same results are obtained for all catalysts regarding the distillation of the feedstock. As selectivity of the catalysts is a key parameter in evaluating the performance of the catalyst, PONA (paraffins (P), olefins (O), naphthenes (N) and aromatics (A) content) of the feedstock and products (after the first 24 h) of each catalyst was investigated. As shown in Fig. 12, all examined catalysts have provided the same products with almost minor differences. However, the least amount of paraffins was obtained for NiMo/G1 and the lowest amount of naphthenes and aromatics was obtained by using the NiMo/G3 sample.

Equation 1 was utilized to calculate the catalytic conversion of sulfur and nitrogen compounds in heavy naphtha. In this respect, HDS and HDN activity of the catalysts was obtained compared to

$$X_i = \left(\frac{c_{i_0} - c_i}{c_{i_0}} \right) \times 100 \quad (1)$$

where X_i indicates the conversion (%) of each compound in the feedstock which includes total sulfur (TS), R-SH compounds (mercaptans) and total nitrogen (TN), c_{i_0} corresponds to the initial concentration of TS, R-SH and TN in the feedstock (ppm), and c_i is related to the concentration of compounds after hydrotreating (ppm).

The performance of the catalysts was investigated in terms of total sulfur conversion, R-SH compound conversion and total nitrogen conversion. Regarding the conversion of sulfur compounds and reduction of the total sulfur, supporting the NiMo over nanoporous graphene has considerably increased the performance. As shown in Fig. 13, the TS conversion for NiMo/G1, NiMo/G2 and NiMo/G3 was increased

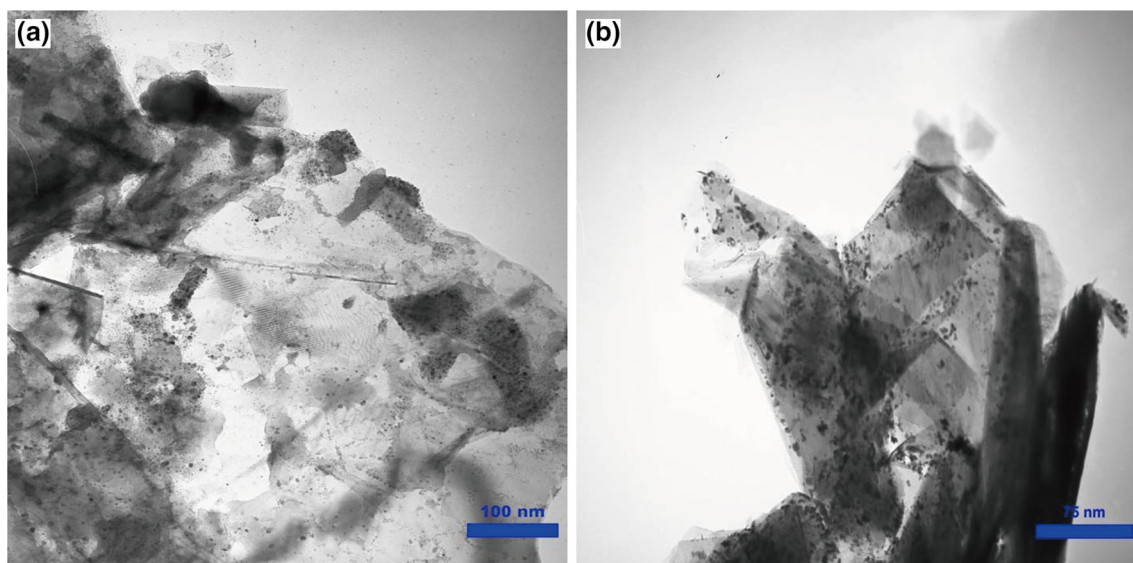


Fig. 10 TEM images of the NiMo/G3 sample

Table 4 Feedstock (heavy naphtha) specifications

Analysis items	Values	Test method
Specific gravity at 15 °C	0.7435	ASTM D4052
Total sulfur, ppm	280	ASTM D5453
R-SH, ppm	51.4	ASTM D3227
Total nitrogen, ppm	3.5	ASTM D4629
RON	45.6	ASTM D2699

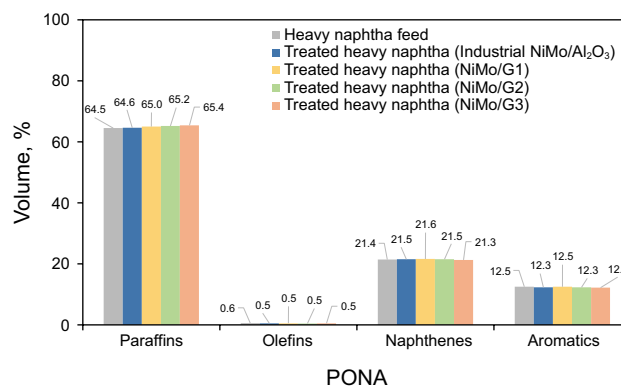


Fig. 12 PONA of heavy naphtha in feedstock and product of all catalysts

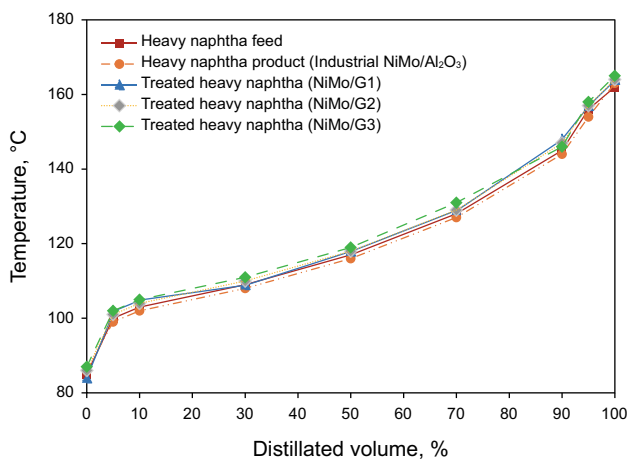


Fig. 11 ASTM D-86 of heavy naphtha in feedstock and product of all catalysts

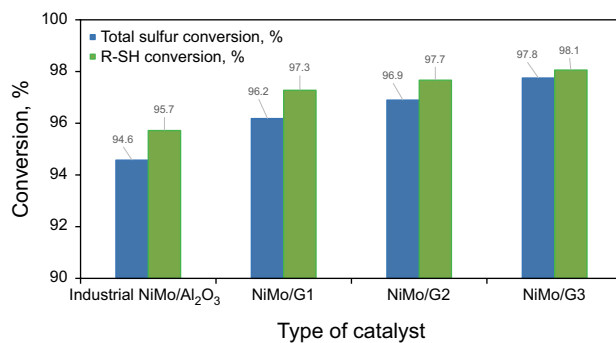


Fig. 13 Catalytic performance of the prepared catalyst in HDS reactions

by 0.6%, 2.3% and 3.2%, respectively, compared with that of the industrial NiMo/alumina catalyst. This can be due to better dispersion of the NiMo active sites over the graphene, which has higher S_{BET} and pore volume. However, different functionalized graphene supports have yielded different results. The best result is obtained for the graphene support that was functionalized by amine followed by acid vapor and carboxylic liquid. Comparing NiMo/G1 and NiMo/G2 reveals that the acid vapor treatment for functionalizing provides better results that can be attributed to the uniform exposure of the graphene to functionalizing agents. Furthermore, as mentioned earlier, the graphene sample functionalized with amine had a higher affinity for metal loading which is indeed effective in catalytic activity. The highest surface area and total pore volume of the NiMo/G3 sample also contributed to its highest activity among the studied catalysts. So the highest activity of the NiMo/G3 sample in terms of sulfur compound conversion can be assigned to its surface properties, highest affinity toward metal loading and probably better distribution of the active sites over the nanoporous graphene. Furthermore, it is reported that incorporating nitrogen into carbon structures enhances their capability for adsorption of sulfur-containing compounds (Adib et al. 2000; Yu et al. 2015, 2016). In addition, it is shown that nitrogen doping of the mesoporous carbon enhances the HDS activity of MoS_2 (Hu et al. 2016), indicating the positive role of incorporating nitrogen into carbon structures. Therefore, the amine agent, which contains nitrogen atoms, might increase the interaction between the catalyst and the heavy naphtha components that is the first step in catalytic reactions.

Removal of the R-SH compounds from the feedstock was enhanced by supporting the NiMo over nanoporous graphene as well. The same trend was obtained for the T-SH conversion, and the NiMo/G3 sample yielded the best result, again followed by NiMo/G2 and NiMo/G1. This is also due to the better metal loading affinity of the amine-functionalized

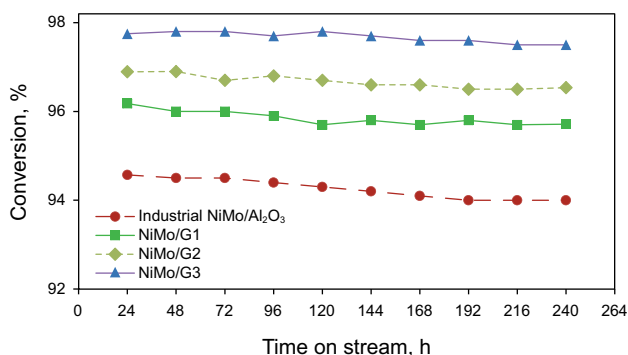


Fig. 14 Conversion of total sulfur of heavy naphtha over different catalysts (reaction conditions: $T=290\text{ }^{\circ}\text{C}$, $P=3.0\text{ MPa}$, $LHSV=3.3\text{ h}^{-1}$ and $H_2/HC=100\text{ NL/L}$)

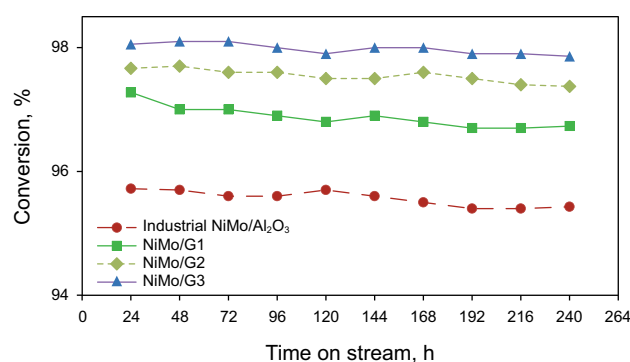


Fig. 15 Conversion of R-SH compounds of heavy naphtha over different catalysts (reaction conditions: $T=290\text{ }^{\circ}\text{C}$, $P=3.0\text{ MPa}$, $LHSV=3.3\text{ h}^{-1}$ and $H_2/HC=100\text{ NL/L}$)

Table 5 Total nitrogen of the treated heavy naphtha by different catalysts

Analysis item	Treated heavy naphtha over different catalysts				Test method
	Industrial NiMo/ Al_2O_3	NiMo/G1	NiMo/G2	NiMo/G3	
Total nitrogen, ppm	< 0.5	< 0.5	< 0.5	< 0.5	ASTM D 4629

graphene and distribution of the active sites over nanoporous graphene. In addition, the time on stream activity of the catalysts in removing the sulfur compounds and R-SH compounds is shown in Figs. 14 and 15.

The NiMo/Gx nanocatalysts were also more active in removing the nitrogen compounds of the heavy naphtha. In this regard, the samples treated with NiMo/alumina, NiMo/G1, NiMo/G2 and NiMo/G3 contained less than 0.5 ppm nitrogen compounds (Table 5).

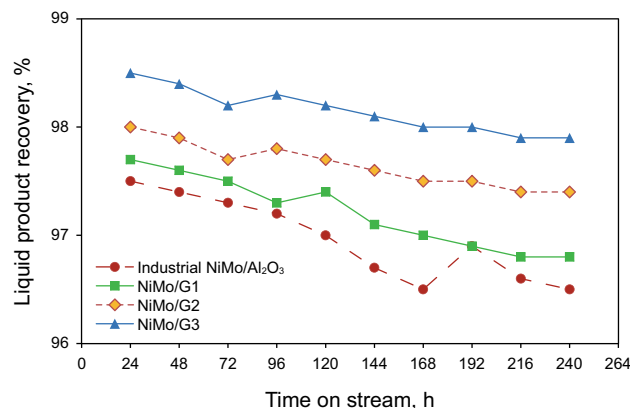


Fig. 16 Liquid product recovery for different catalysts

Liquid recovery of the prepared catalysts along with that of the NiMo/alumina industrial catalyst is shown in Fig. 16. It is observed that after 240 h of hydrotreating, the highest liquid recovery was obtained for the NiMo/G3 nanocatalyst once more.

4 Conclusion

In this research, NiMo supported on nanoporous graphene catalysts was prepared by using functionalized nanoporous graphene. The nanoporous graphene support was functionalized through liquid treatment for carboxylic function, acid gas treatment for carboxylic function and acid gas treatment for amine functionalizing. In the following, the effect of the functionalizing method on HDS and HDN activity of the catalysts was studied. It was observed that all NiMo/Gx catalysts had much better performance compared with the NiMo/alumina industrial catalyst. Regarding the removal of sulfur compounds and total sulfur reduction, the sample prepared with amine-functionalized graphene (NiMo/G3) showed better results (i.e., 97.8% TS conversion), followed by NiMo/G2 and NiMo/G1. In addition, the NiMo/G3 sample provided the highest R-SH conversion (i.e., 98.1%) confirming its great performance in hydrotreating the heavy naphtha. The best performance of the amine-functionalized in HDS and HDN of the heavy naphtha is attributed to its better surface properties, the higher affinity of the amine-functionalized graphene toward metal loading and higher interaction between amine-functionalized support and sulfur components of the heavy naphtha.

Open Access This article is distributed under the terms of the Creative Commons Attribution 4.0 International License (<http://creativecommons.org/licenses/by/4.0/>), which permits unrestricted use, distribution, and reproduction in any medium, provided you give appropriate credit to the original author(s) and the source, provide a link to the Creative Commons license, and indicate if changes were made.

References

- Adib F, Bagreev A, Bandosz TJ. Adsorption/oxidation of hydrogen sulfide on nitrogen-containing activated carbons. *Langmuir*. 2000;16(4):1980–6. <https://doi.org/10.1021/la990926o>.
- Andonova S, Vladov C, Pawelec B, Shtereva I, Tyuliev G, Damyanova S, et al. Effect of the modified support γ -Al₂O₃-CaO on the structure and hydrodesulfurization activity of Mo and Ni–Mo catalysts. *Appl Catal A Gen*. 2007;328(2):201–9. <https://doi.org/10.1016/j.apcata.2007.06.009>.
- Ayala-Gomez M, Puello-Polo E, Quintana P, González-García G, Diaz C. Comparison between alumina supported catalytic precursors and their application in thiophene hydrodesulfurization:(NH₄)₄[NiMo₆O₂₄H₆]·5H₂O/ γ -Al₂O₃ and NiMoOx/ γ -Al₂O₃ conventional systems. *RSC Adv*. 2015;5(124):102652–62. <https://doi.org/10.1039/c5ra17695f>.
- Bell W, Dietz S. Mesoporous carbons and polymers. Google Patents; 2001.
- Bui NQ, Geantet C, Berhault G. Maleic acid, an efficient additive for the activation of regenerated CoMo/Al₂O₃ hydrotreating catalysts. *J Catal*. 2015;330:374–86. <https://doi.org/10.1016/j.jcat.2015.07.031>.
- Bunch AY, Ozkan US. Investigation of the reaction network of benzofuran hydrodeoxygenation over sulfided and reduced Ni–Mo/Al₂O₃ catalysts. *J Catal*. 2002;206(2):177–87. <https://doi.org/10.1006/jcat.2001.3490>.
- Dhar GM, Srinivas BN, Rana MS, Kumar M, Maity SK. Mixed oxide supported hydrodesulfurization catalysts—A review. *Catal Today*. 2003;86(1–4):45–60. [https://doi.org/10.1016/S0920-5861\(03\)00403-6](https://doi.org/10.1016/S0920-5861(03)00403-6).
- Escobar J, Barrera MC, Gutiérrez AW, Terrazas JE. Benzothiophene hydrodesulfurization over NiMo/alumina catalysts modified by citric acid. Effect of addition stage of organic modifier. *Fuel Process Technol*. 2017;156:33–42. <https://doi.org/10.1016/j.fuproc.2016.09.028>.
- Gutiérrez OY, Singh S, Schachtl E, Kim J, Kondratieva E, Hein J, et al. Effects of the support on the performance and promotion of (Ni)MoS₂ catalysts for simultaneous hydrodenitrogenation and hydrodesulfurization. *ACS Catal*. 2014;4(5):1487–99. <https://doi.org/10.1021/cs500034d>.
- Hajjar Z, Kazemeini M, Rashidi A, Bazmi M. In situ and simultaneous synthesis of a novel graphene-based catalyst for deep hydrodesulfurization of naphtha. *Catal Lett*. 2015;145(9):1660–72. <https://doi.org/10.1007/s10562-015-1563-y>.
- Hajjar Z, Kazemeini M, Rashidi A, Bazmi M. Graphene based catalysts for deep hydrodesulfurization of naphtha and diesel fuels: a physicochemical study. *Fuel*. 2016;165:468–76. <https://doi.org/10.1016/j.fuel.2015.10.040>.
- Hajjar Z, Kazemeini M, Rashidi A, Soltanali S, Bahadoran F. Naphtha HDS over Co–Mo/graphene catalyst synthesized through the spray pyrolysis technique. *J Anal Appl Pyrolysis*. 2017;123:144–51. <https://doi.org/10.1016/j.jaap.2016.12.013>.
- Hu J, Zhang Z, Wang F, Zheng S, Cai J, Qin J, et al. A controllable synthesis of nitrogen-doped mesoporous carbon supported MoS₂ catalysts for hydrodesulfurization of thiophene. *RSC Adv*. 2016;6(103):101544–51. <https://doi.org/10.1016/j.apcata.2007.06.009>.
- Khorami P, Kalbasi M. Hydrodesulphurisation activity of CoMo catalyst supported on multi wall carbon nanotube: sulphur species study. *J Exp Nanosci*. 2011;6(4):349–61. <https://doi.org/10.1080/17458080.2010.497948>.
- Liu H, Li Y, Yin C, Wu Y, Chai Y, Dong D, et al. One-pot synthesis of ordered mesoporous NiMo–Al₂O₃ catalysts for dibenzothiophene hydrodesulfurization. *Appl Catal B Environ*. 2016;198:493–507. <https://doi.org/10.1016/j.apcatb.2016.06.004>.
- Liu N, Wang X, Xu W, Hu H, Liang J, Qiu J. Microwave-assisted synthesis of MoS₂/graphene nanocomposites for efficient hydrodesulfurization. *Fuel*. 2014;119:163–9. <https://doi.org/10.1016/j.fuel.2013.11.045>.
- Mendoza-Nieto JA, Robles-Méndez F, Klimova TE. Support effect on the catalytic performance of trimetallic NiMoW catalysts prepared with citric acid in HDS of dibenzothiophenes. *Catal Today*. 2015;250:47–59. <https://doi.org/10.1016/j.cattod.2014.05.002>.
- Nikulshin PA, Salnikov VA, Mozhaev AV, Minaev PP, Kogan VM, Pimerzin AA. Relationship between active phase morphology and catalytic properties of the carbon–alumina-supported Co(Ni)Mo catalysts in HDS and HYD reactions. *J Catal*. 2014;309(1–2):386–96. <https://doi.org/10.1016/j.jcat.2013.10.020>.
- Purón H, Pinilla JL, de la Fuente JAM, Millán MG. Effect of metal loading in NiMo/Al₂O₃ catalysts on Maya vacuum residue hydrocracking. *Energy Fuels*. 2017;31(5):4843–50. <https://doi.org/10.1021/acs.energyfuels.7b00104>.

- Saih Y, Nagata M, Funamoto T, Masuyama Y, Segawa K. Ultra deep hydrodesulfurization of dibenzothiophene derivatives over NiMo/TiO₂-Al₂O₃ catalysts. *Appl Catal A Gen.* 2005;295(1):11–22. <https://doi.org/10.1016/j.apcata.2005.07.024>.
- Santes V, Herbert J, Cortez MT, Zárate R, Díaz L, Medellín B. Hydro-treating activity of heavy gasoil over NiMo/ γ -Al₂O₃-TiO₂. *Pet Sci Technol.* 2004;22(1–2):103–17. <https://doi.org/10.1081/LFT-120028526>.
- Soghrati E, Kazemeini M, Rashidi AM, Jozani KJ. Preparation and characterization of Co–Mo catalyst supported on CNT coated cordierite monoliths utilized for naphtha HDS process. *Proc Eng.* 2012;42:1484–92. <https://doi.org/10.1016/j.proeng.2012.07.541>.
- Vonortas A, Papayannakos N. Kinetic Study of the hydrodesulfurization of a heavy gasoil in the presence of free fatty acids using a CoMo/ γ -Al₂O₃ catalyst. *Ind Eng Chem Res.* 2014;53(23):9646–52. <https://doi.org/10.1021/ie5006492>.
- Wang H, Xiao B, Cheng X, Wang C, Zhao L, Zhu Y, et al. NiMo catalysts supported on graphene-modified mesoporous TiO₂ toward highly efficient hydrodesulfurization of dibenzothiophene. *Appl Catal A Gen.* 2015;502:157–65. <https://doi.org/10.1016/j.apcata.2015.05.028>.
- Xu J, Huang T, Fan Y. Highly efficient NiMo/SiO₂-Al₂O₃ hydrodesulfurization catalyst prepared from gemini surfactant-dispersed Mo precursor. *Appl Catal B Environ.* 2017;203:839–50. <https://doi.org/10.1016/j.apcatb.2016.10.078>.
- Yu Z, Wang X, Song X, Liu Y, Qiu J. Molten salt synthesis of nitrogen-doped porous carbons for hydrogen sulfide adsorptive removal. *Carbon.* 2015;95:852–60. <https://doi.org/10.1016/j.carbon.2015.08.105>.
- Yu Z, Wang X, Zhou S, Yang L, Zhao Z, Qiu J. A facile soft-template synthesis of nitrogen doped mesoporous carbons for hydrogen sulfide removal. *Adsorption.* 2016;22(8):1075–82. <https://doi.org/10.1007/s10450-016-9823-8>.
- Zdražil M. MgO-supported Mo, CoMo and NiMo sulfide hydrotreating catalysts. *Catal Today.* 2003;86(1–4):151–71. [https://doi.org/10.1016/S0920-5861\(03\)00409-7](https://doi.org/10.1016/S0920-5861(03)00409-7).
- Zepeda TA, Pawelec B, Obeso-Estrella R, de León JND, Fuentes S, Alonso-Núñez G, et al. Competitive HDS and HDN reactions over NiMoS/HMS-Al catalysts: diminishing of the inhibition of HDS reaction by support modification with P. *Appl Catal B Environ.* 2016;180:569–79. <https://doi.org/10.1016/j.apcatb.2015.07.013>.
- Zhou W, Liu M, Zhou Y, Wei Q, Zhang Q, Ding S, et al. 4,6-dimethylidibenzothiophene hydrodesulfurization on nickel-modified USY-Supported NiMoS catalysts: effects of modification method. *Energy Fuels.* 2017;31(7):7445–55. <https://doi.org/10.1021/acs.energyfuels.7b01113>.